Ion motion and emission profiles in low-pressure cylindrical discharges

Christopher C. Davis
Electrical Engineering Department, University of Maryland, College Park, Maryland 20742
(Received 28 September 1984; revised manuscript received 17 June 1985)

Ions in a cylindrical, low-pressure gas discharge move in a combination of axial and radial fields. Their motion is predominantly in the radial direction and this motion affects the shape of ion emission lines observed along the discharge-tube axis. Calculations are presented here that show in detail how the ion motion affects these line shapes for a Tonks-Langmuir radial potential with ion mean free paths of various values relative to the tube radius. These calculations predict both values for the axial ion drift velocity and asymmetrical longitudinally emitted line shapes. The predictions of the theory compare well with experimental observations made on argon-ion-laser discharges.

I. INTRODUCTION

In a low-pressure electrical discharge in a cylindrical tube, ions formed in the body of the discharge move under the influence of both longitudinal and radial electric fields. The radial field in such discharges is generally much stronger than the longitudinal one so that the motion of ions from their point of creation is predominantly in the radial direction. This radial motion, when combined with the random component of ion velocity, leads to line profiles observed in the direction perpendicular to the tube axis being broader than profiles observed in the axial direction. Line profiles observed in the axial direction have been generally assumed to reflect the random ion velocity distribution, with a Doppler shift of the line center by an amount corresponding to a uniform longitudinal ion drift velocity. It is our intention in this paper to show that the longitudinally emitted ion line shape does not take this simple form. It is Doppler shifted, but it is also rendered asymmetric because ground-state ions accelerate for different time durations depending on their radial positions at creation and subsequent electron input excitation (and almost immediate emission).

In a cylindrical discharge the longitudinal electric field arises from the externally applied potential and can be assumed to be uniform in the longitudinal direction within the positive column. The radial field results from the negative charge which builds up on the tube walls in order to preserve plasma quasineutrality. Because the electron temperature T_e in such a discharge is much greater than that of the ions, the random electron current to the wall,[1] $eN_e(w)(kT/2\pi m_e)^{1/2}$, where $N_e(w)$ is the electron density at the wall and the other symbols have their usual significance, is much greater than that of the ions. If the average radial drift velocity of ions at the wall is $\bar{v}_r(w)$, then in equilibrium

$$N_e(w)(kT_e/2\pi m_e)^{1/2}=N_i(w)\bar{v}_r(w) , \tag{1}$$

where $N_i(w)$ is the ion density at the wall. In normal circumstances this equation is only satisfied by having $N_i(w)>N_e(w)$. The extent of the sheath region near the wall where this change imbalance occurs is typically of the order of a few Debye lengths. The Debye length λ_{D_0} in SI units is defined by

$$\lambda_{D_0}=[\epsilon_0 kT_e/N_e(0)e^2]^{1/2} , \tag{2}$$

where $N_e(0)$ is the axial electron density. In most low-pressure discharges of practical importance, such as are used to excite noble-gas ion lasers, $\lambda_{D_0}\ll R$, where R is the radius of the discharge tube, so the plasma is quasineutral except very close to the wall.

In the theory of the low-pressure discharge given by Tonks and Langmuir[1] the quasineutral plasma and sheath are treated separately. Outside the sheath the electron density is

$$N_e(r)=N_{e_0}\exp[e\phi(r)/kT_e] , \tag{3}$$

where $\phi(r)$ is the radial distribution of potential in the discharge. The radial variation in ion production $G(r)$ is assumed to be proportional to the electron density

$$G(r)=ZN_e(r) , \tag{4}$$

where Z is the ionization rate (electron-ion pairs produced per second per electron). The ions are assumed to be formed at rest and then fall collisionlessly to the walls where they recombine with electrons and re-enter the discharge as neutral particles. If a group of ions originate in an elementary annulus of width $d\rho$ at radius ρ, their concentration at radius r is

$$N_{\rho r}=G(\rho)(\rho/r)d\rho/v_{\rho r} , \tag{5}$$

where $v_{\rho r}$ is the radial velocity acquired by an ion in moving from radius ρ to radius r, and

$$v_{\rho r}=\left[\frac{2e}{M}[\phi(\rho)-\phi(r)]\right]^{1/2} , \tag{6}$$

where M is the ion mass. The total ion density at radius r is then[2]

$$N_i(r)=\int_0^r N_{\rho r} . \tag{7}$$

Working from these assumptions, Tonks and Langmuir were able to calculate the radial distribution of charged

particles within the plasma, the radial potential distribution, and the parametric variation of the electron temperature. However, they treat the space-charge sheath near the discharge-tube wall separately from the quasineutral plasma and attempt to match their solutions for sheath and plasma at the sheath boundary. To describe the whole region of plasma and sheath more exactly a single solution for $N_e(r)$ and $\phi(r)$ should be found. In cylindrical geometry this has been done by Forrest and Franklin.[3] The assumption of quasineutrality in the plasma is abandoned, although in practice the actual deviation from quasineutrality is negligible outside the sheath region. Forrest and Franklin[3,4] characterize the plasma by two parameters α and δ^*, where

$$\alpha^2=\frac{\epsilon_0 Z^2 M_i}{N_{e_0} e^2}=\frac{\lambda_{D_0}^2 Z^2 M_i}{kT_e} \tag{8}$$

and

$$\delta^*=\frac{kT_e}{2ZM_i D_e}+\frac{\nu_i}{2Z}\ , \tag{9}$$

where M_i is the ion mass, D_e is the diffusion coefficient of the electrons, and ν_i is the collision frequency of the ions for (momentum plus charge) transfer. α is a measure of the extent to which space-charge effects are important in the plasma, a small value of α implies that quasineutrality is obeyed within the plasma. Complete neutrality corresponds to $\alpha=0$; for large values of α ($>10^{-2}$) the boundary between the quasineutral plasma and the space charge becomes ill-defined and the assumption of bulk quasineutrality within the plasma is no longer valid. In a typical argon-ion-laser discharge plasma α is estimated to be $\sim 10^{-8}$ (Ref. 5), so the assumption of bulk quasineutrality is very reasonable. If in addition the flow of ions to the wall is indeed collisionless, then the factor δ^* is zero and Tonks-Langmuir theory should provide a very adequate description of the plasma. In this case the radial electron density distribution can be written in the form[6]

$$N_e(r)=N_{e_0}\exp(-1.155\{1-[1-(r/R)^2]^{1/2}\}) \tag{10}$$

and the radial potential distribution as

$$\phi(r)=\frac{1.155kT_e}{e}\{1-[1-(r/R)^2]^{1/2}\}\ . \tag{11}$$

If ions undergo collisions on their way to the wall, then Tonks-Langmuir (TL) theory will no longer hold, although in practice for an ion mean free path $\gtrsim R$ the deviation of $N_e(r)$ and $\phi(r)$ from the forms given by Eqs. (10) and (11) should be relatively small.

As pointed out by Valentini in a series of papers,[7–9] considerable deviation of the radial electron density and potential from the forms given by Eqs. (10) and (11) will occur if the plasma is highly ionized, as this depletes the neutral-atom density on axis. Additional complications also can arise produced by directed motion of neutral atoms leaving the wall if the ion flux at the wall becomes large enough.[9,10]

Thus, the focus in this paper will be on low-pressure discharge plasmas without applied external magnetic field where the theory originally formulated by Tonks and Langmuir holds. Several authors[3,4,7–9,11,12] have confirmed the correctness of this theory in the close-to-collisionless regime where the degree of ionization is not too high. For practical purposes, the conditions for Tonks-Langmuir theory to hold have been demonstrated experimentally by Webb.[13] He has shown that for values of the product $p_0 R \leq 0.4$ Torr mm (where p_0 is the pressure in the tube after thermal driveout[5]) that the radial-ion-density profile follows that predicted by Tonks-Langmuir theory. This, surprisingly, corresponds to an ion-mean-free-path—to—tube-radius ratio of only about 0.1.

The ion dynamics which result from combined radial and longitudinal motion have very interesting effects on the emission profiles of ion transitions observed from such a discharge. In practice, discharge plasmas where such effects might be expected to be observed occur in the noble-gas ion lasers, where current densities up to several million amps/m^2 are passed through gases at low-number densities (typically 3×10^{22} m^{-3}). It has been common practice to observe the emission profiles of ion transitions in such plasmas and thereby to deduce several parameters of the plasma, such as the electron and ion temperatures, and the radial and longitudinal ion velocities. Much of the diagnostic information about these plasmas has been derived from experimental observations by the use of formulas derived by Kagan and Perel.[14–17] Kitaeva and her co-workers have done considerable work in this area.[18,19]

II. TRANSVERSELY EMITTED ION LINE SHAPES

The predominant radially directed motion of the ions in a low-pressure cylindrical discharge, when combined with the random component of ion velocity (usually assumed to belong to a Maxwellian distribution), leads to line profiles observed in the transverse direction being broader than profiles observed in the axial direction. This fact has led numerous investigators[14–21] to deduce plasma parameters such as electron, ion, and neutral-atom temperatures, and average directed ion velocities from transverse and axial line-shape observations.

In the simplest model, the transversely emitted profile is assumed to be a superposition of two Gaussian profiles, one blue shifted by a constant radial velocity, which comes from ions in the near half of the tube bore, and one red shifted by a constant radial velocity, which comes from ions in the far half of the tube bore.[20]

Kagan and Perel[14–17] perform a more realistic analysis of the problem, in so far as they attempt to determine the distribution of ion velocities including both longitudinal and transverse ion drifts. However, simplifying assumptions about the form of these distributions are made to simplify the analysis, and as a consequence the final relationships between measured linewidth and various plasma parameters are in error. Sze and Bennett[21] made a subsequent study of the effect of transverse ion motion on observed line shapes and were able to correct the formulas of Kagan and Perel to more exactly relate the plasma parameters T_a (the neutral-atom temperature) and T_e (the elec-

tron temperature) to observed transverse line shapes. The observed transverse ion temperature T^*, measured by assuming that the transversely emitted line shape results from a one-dimensional Maxwellian distribution, is[21]

$$T^* = 0.716T_a + 0.21T_e \ . \tag{12}$$

However, it should be pointed out that even this relationship depends to some extent on the geometrical arrangement in which radiation emitted in the transverse direction from the cylindrical plasma is collected.

A better treatment of radial ion motion in the collisionless regime has been given by Zakharov and Pekar[22] who integrate the Boltzmann equation for the ion distribution function numerically and obtain the expression

$$T^* = 0.64T_a + 0.118T_e \ . \tag{13}$$

Unfortunately, their final averaging in the radial direction makes the same error as Kagan and Perel[15] and pointed out by Sze and Bennett:[21] namely, the average over radially directed velocities should be[21]

$$\overline{v_\rho^2} = \frac{\int_0^R n_i v_\rho^2 n_e \rho \, d\rho}{\int_0^R n_i n_e \rho \, d\rho} \ , \tag{14}$$

where $v_\rho(\rho)$ is the radially directed velocity, and n_i, n_e are the radially dependent ion and electron densities, respectively. Averaging of the form[16,23]

$$\overline{v_\rho^2} = \frac{\int_0^R n_i v_\rho^2 n_e \, d\rho}{\int_0^R n_i n_e \, d\rho} \tag{15}$$

does not take into account the cylindrical symmetry of the situation.

III. LONGITUDINALLY EMITTED ION LINE SHAPES

The simplest assumption that has been made in analyzing the longitudinally emitted line shape is that it has a Doppler width that reflects the true ion temperature in the discharge and a center frequency which is Doppler shifted by an amount

$$\Delta\nu_z = v_z \nu_0 / c \ , \tag{16}$$

where v_z is the directed axial velocity in the direction of observation associated with the peak of the ion velocity distribution in the z direction. It has been standard practice to assume that v_z is independent of radial location within the discharge cross section. Indeed, it is not always clear whether published observations of axially emitted line shapes involve light collection from the whole, or a part, of the tube cross section.

By this means, supposedly correct values for the ion temperature T_i can be determined. This generally involves unfolding the Lorentzian contribution from the Voigt profiles which have been assumed to be emitted in the axial direction. It is our intention in this paper to show that the ion motion in the longitudinal direction is not so straightforward as is implied by Eq. (16). Indeed, under appropriate conditions, asymmetrical line shapes should be observed in the axial direction. These asymmetries have nothing to do with asymmetries which might be observed if emitted ions could be significantly accelerated during their radiative lifetime.[23] The neglect of the full effects of longitudinal ion motion might well explain the very large discrepancies between the Lorentzian widths estimated from axially emitted ion line profiles by different investigators.[22–29]

In the model to be considered here ions are assumed to be produced from neutral atoms at a rate proportional to local electron density and then move in the combined radial and longitudinal electric fields in the positive column. Excited ions are produced by electron collisions predominantly on ground-state ions so their excitation from the neutral-atom ground state is a two-step process. However, the excited ion lifetimes associated with levels that are usually observed for diagnostic purposes are very short [10 ns or less (Ref. 5)], so there is negligible change in ion velocity during the time the ion is excited. Thus, the line shapes observed from excited ions reflect the velocity distribution of the ion ground state. If ions were excited directly from neutrals by a single electron collision their line shapes would reflect the neutral-atom velocity distribution. It is assumed that the neutral atoms have no memory of previous ionization and charge exchange neutralization so that their velocity is Maxwellian distributed about zero. We shall consider the case where the ions move both collisionlessly and with collisions to the tube wall. A collision will be assumed to produce a new ion with no net directed velocity. In this model, ions at radius r, where $0 \le r \le R$, can have different acquired longitudinal velocities depending on the radial position ρ where they originated, where $0 \le \rho \le r$. The largest longitudinal velocity is acquired by ions which have drifted collisionlessly from the tube axis. We shall assume that the net ion motion is still predominantly radially directed so the probability of a given ion making a collision is purely a function of the radial distance it has traveled, $r - \rho$. This assumption is justified in more detail in the Appendix. We shall also assume that the degree of ionization in the discharge is sufficiently low that neutral-atom depletion and directed velocity effects can be neglected.

IV. RADIAL VARIATION OF LONGITUDINAL DRIFT VELOCITY

In this section we shall derive quantitative expressions for the radial variation in longitudinal ion drift velocity. This variation results because ions which are excited from the ground state to a short-lived emitting level have an acquired longitudinal velocity that depends on the radial position where the ground-state ion was originally formed and the final radial position where the ion is excited from the ground state (and almost immediately emits).

A. Collisionless regime

If the radial potential function is $\phi(r')$, an ion moving from its point of creation ρ to radius r acquires a longitudinal velocity

$$v_{z\rho r} = \frac{eE_{\|}}{M} \int_\rho^r \frac{1}{v_{\rho r'}} dr' \ , \tag{17}$$

where $E_{\|}$ is the longitudinal electric field. Thus the average longitudinally directed velocity at radius r is

$$v_{zr}=\int_0^r \frac{G(\rho)v_{z\rho r}\rho}{N_i(r)rv_{\rho r}}d\rho \ . \tag{18}$$

Equation (18) is most easily evaluated by rewriting it in dimensionless form with $\rho/R=x$, $v/R=a$, and using a dimensionless radial potential

$$V(x)=e\phi(x)/kT_e \ .$$

For certain forms of the radial potential Eq. (18) can be written in a simpler form. For an assumed linear variation in radial potential of the form

$$V_x=-V_0x \ , \tag{19}$$

the radial variation in longitudinal drift velocity is

$$v_{zr}=\frac{eE_{\|}R}{M}\left[\frac{M}{2kT_e}\right]^{1/2}f(a,V_0)=Af(a,V_0) \ , \tag{20}$$

where

$$f(a,V_0)=\frac{1}{V_0^2}[1-(1+V_0a)e^{-V_0}]/\{[a+1/(2V_0)]F((V_0a)^{1/2})-\tfrac{1}{2}(a/V_0)^{1/2}\} \tag{21}$$

and $F(z)$ is Dawson's integral[23,30]

$$F(z)=e^{-z^2}\int_0^z e^{t^2}dt \ . \tag{22}$$

For a quadratic potential (which approximates the TL potential near the tube axis) of the form

$$V_x=-V_0x^2 \ , \tag{23}$$

the radial variation in longitudinal drift velocity is

$$V_{zr}=Ag(a) \ , \tag{24}$$

where

$$g(a)=\frac{a}{F((V_0a^2)^{1/2})}\int_0^\infty \frac{y\exp(V_0a^2\tanh^2y)}{\cosh^2y}dy \ . \tag{25}$$

The limiting value for the longitudinal drift velocity on axis is

$$v_{z0}=\frac{eE_{\|}R}{M}\left[\frac{M}{2kT_eV_0}\right]^{1/2}\ln 2 \tag{26}$$

which will later be seen to be a physically realistic value, in contrast to the zero axial drift velocity predicted by Eq. (20).

Using the relation given by Forrest and Franklin[4]

$$R\left[\frac{M}{kT_e}\right]^{1/2}=\frac{1.109}{Z} \ , \tag{27}$$

where Z is the ionization rate in the discharge, the longitudinal drift velocity on axis can be written as

$$v_{z0}=1.032\frac{eE_{\|}}{M}\frac{\ln 2}{Z} \ , \tag{28}$$

a result in extremely close agreement with one derived by Kagan and Perel.[14]

For the TL potential given by Eq. (11), Eq. (18) can be written explicitly as

$$v_{zr}=\frac{eE_{\|}R}{M}\left[\frac{M}{2.31kT_e}\right]^{1/2}\frac{\int_0^a dx\dfrac{xe^{V_x}}{[(1-x^2)^{1/2}-(1-a^2)^{1/2}]^{1/2}}\int_x^a dy\dfrac{1}{[(1-x^2)^{1/2}-(1-y^2)^{1/2}]^{1/2}}}{\int_0^a dx\dfrac{xe^{V_x}}{[(1-x^2)^{1/2}-(1-a^2)^{1/2}]^{1/2}}} \ . \tag{29}$$

These integrals are written out in full so that the principal problem in their numerical evaluation can be pointed out. Depending on the value of a, these elliptic integrals blow up at one or both endpoints. They were evaluated by numerical integration, except near the endpoints where analytical expressions for the contribution to the integrands were used. The accuracy of this integration procedure was checked by determining the axial drift velocity and comparing it with the analytic value determined from (26), which is

$$v_{zr}=(A\ln 2)(2/1.155)^{1/2} \ . \tag{30}$$

The integration procedure used gave this result with high precision if long computational time was allowed. Because many points were required, the computational accuracy required was relaxed to 1% to reduce computation time.

The longitudinal drift velocity averaged over the tube bore is

$$\bar{v}_z = \frac{\int_0^R dr\, r \int_0^r d\rho\, N_{\rho r} v_{z\rho r}}{\int_0^R dr\, r \int_0^r d\rho\, N_{\rho r}} \tag{31}$$

which is determined numerically by similar procedures to those described for Eq. (29).

B. With collisions

We assume that the mean free path λ for drifting ions is independent of their velocity and again assume that the predominant motion is radially directed. With these assumptions the probability of an ion originating at radius ρ and reaching radius r is $\exp[-(r-\rho)/\lambda]$. Thus, in contrast with Eq. (5),

$$N_{\rho r} = G(\rho)(\rho/r)\exp[-(r-\rho)/\lambda]d\rho/v_{\rho r}\ . \tag{32}$$

The radial variation in longitudinal drift velocity becomes, therefore,

$$v_{zr} = A \frac{\int_0^a dx \dfrac{x \exp\left[V_x - \dfrac{R}{\lambda}(a-x)\right]}{(V_x - V_a)^{1/2}} \int_x^a dy \dfrac{1}{(V_x - V_y)^{1/2}}}{\int_0^a dx \dfrac{x \exp\left[V_x - \dfrac{R}{\lambda}(a-x)\right]}{(V_x - V_a)^{1/2}}}\ . \tag{33}$$

For a linear potential

$$v_{zr} = \frac{A}{V_0^2}\left[\frac{V_0}{V_0'}\right]^{3/2} f(x, V')\ , \tag{34}$$

where $V_0' = |V_0 - R/\lambda|$ and $f(x, V_0')$ is of the form given by Eq. (21).

For a quadratic potential

$$v_{zr} = Ah(x)\ , \tag{35}$$

where

$$h(x) = \frac{\dfrac{x}{V_0^{1/2}} \int_0^\infty dy \left[y \exp\left[-\dfrac{V_0 x^2}{\cosh^2 y} + \dfrac{Rx}{\lambda \cosh y}\right]\dfrac{1}{\cosh y}\right]}{\int_0^a dy \dfrac{y \exp\left[-V_0 y^2 + \dfrac{Ry}{\lambda}\right]}{(x^2 - y^2)^{1/2}}} \tag{36}$$

which presents no problems in numerical evaluation. On axis the longitudinal drift velocity reduces to Eq. (26).

For a TL potential Eq. (33) can be evaluated numerically by similar techniques to those described in the collisionless case. The longitudinal drift velocity averaged over the tube bore is evaluated from Eq. (31).

C. Results and discussion

The radial variation of longitudinal drift velocity for linear, quadratic, and TL potentials is shown in Figs. 1–3 for both the collisionless case and for various nonzero values of the collision factor R/λ. The results for the linear potential probably do not have any practical significance but are included for completeness. The quadratic and TL potentials give identical results near the axis and both show significant radial variations in drift velocity. Interestingly enough, for values of $R/\lambda \sim 0.5$ this radial variation becomes quite small except close to the tube walls (where some of the assumptions of the model may break down in any case). Curves for values of $R/\lambda > 2$ are not to be taken too seriously as the use of a TL potential will cease to be a good approximation in this case.

Numerical values of longitudinal drift velocities calculated from Eq. (33) and averaged over the tube bore are in good agreement with measured values of $E_{||}$ and T_e obtained for argon discharges. For example, Fig. 4 shows the calculated variation in $\bar{v}_z$ in units of A with collision factor R/λ for a TL potential. The value of A is

$$A = \frac{eE_{||}R}{M}\left[\frac{M}{2kT_e}\right]^{1/2} \tag{37}$$

in units of m/s. For a typical argon ion laser with $R = 1$ mm, $kT_e = 2.5$ eV, and $E_{||} = 300\ \mathrm{V\,m^{-1}}$, $A = 208$ m/s. With $R/\lambda = 1$ the calculated value of $\bar{v}_z$ is 189 m/s. Under these conditions Ballik *et al.*[24] measure $\bar{v}_z \simeq 170$ m/s with a small variation with pressure. In larger-bore discharge tubes, measured longitudinal drift velocities tend to be slightly lower. This is consistent with a reduction of $E_{||}$ in larger tubes, an increase in the collision factor R/λ, and electron temperatures which are slightly lower (under equivalent conditions of current density and pressure). The pressure variation is quite consistent with (i) the variation of $E_{||}$ with pressure, with $E_{||}$ generally falling as the pressure decreases, and (ii) the variation of $\bar{v}_z$ with R/λ. The latter variation is surprisingly small until pressures outside the normal operating regime of argon ion lasers are reached. Most of these lasers operate with $R/\lambda \sim 1$. Webb has concluded that the mean free

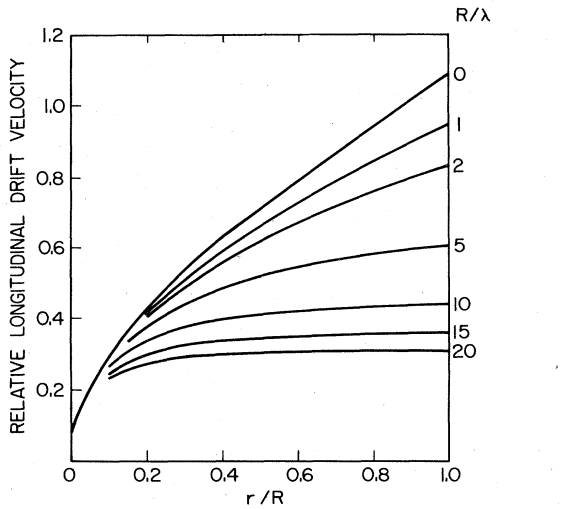

FIG. 1. Radial variation in longitudinal ion drift velocity in a cylindrical discharge with a linear radial potential, for various values of the collision factor R/λ. R is the tube radius and λ the ion mean free path.

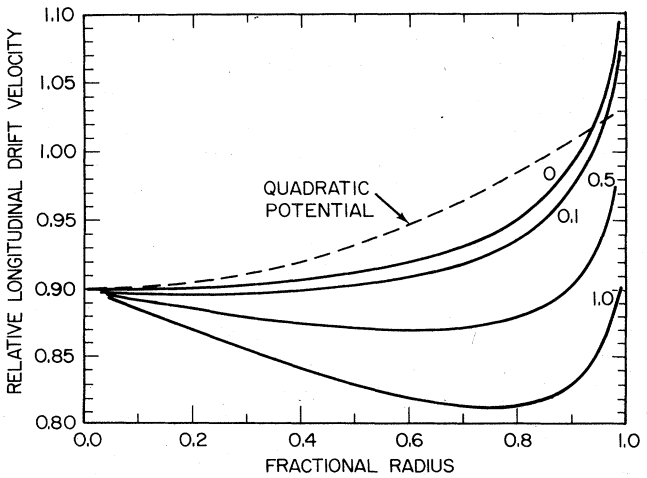

FIG. 2. Radial variation in longitudinal ion drift velocity in a cylindrical discharge with a Tonks-Langmuir radial potential, for various values of R/λ, shown on each curve. The collisionless case for a quadratic radial potential is also shown normalized to the same axial velocity as the other curves.

path of the predominantly radially moving argon ions follows the formula

$$\lambda_i = 3.3\times 10^{-5}/p_0 \text{ m} , \tag{38}$$

where p_0 is the *effective* filling pressure in Torr in the discharge region. Typical *effective* filling pressures, after thermal driveout, are $\sim 0.05-0.1$ Torr. The work of several different investigators, which has been summarized by Davis and King,[5] is entirely consistent with the predictions of Eq. (31). It is our belief that the predictions of this theory together with measurement of the electric field in the positive column and the ion drift velocity represent the most reliable method for determining electron temperatures in low-pressure cylindrical plasmas. This is particularly true given the difficulty of obtaining reliable and reproducible data with probes, particularly in narrow-bore discharges where they constitute a severe perturbation of the plasma.

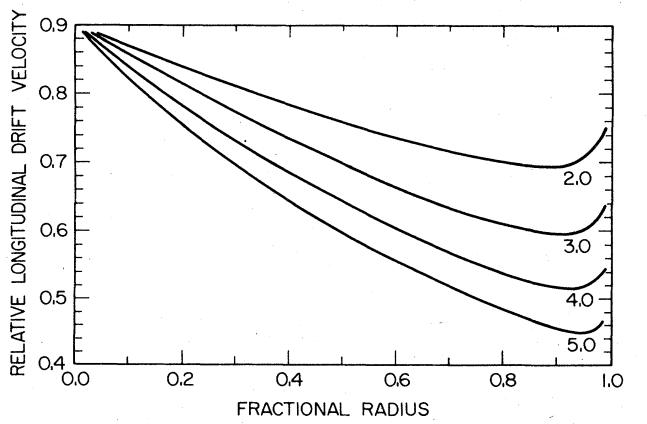

FIG. 3. Radial variation in longitudinal ion drift velocity in a cylindrical discharge with a Tonks-Langmuir radial potential, for various values of R/λ, shown on each curve.

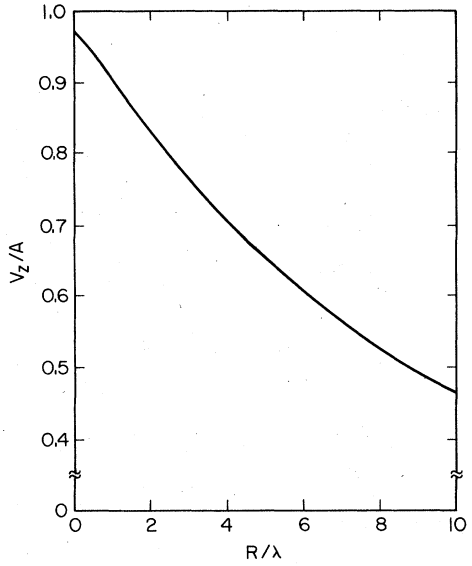

FIG. 4. Normalized longitudinal ion drift velocity averaged over the tube bore for a cylindrical plasma with a Tonks-Langmuir radial potential, for various values of the collision factor R/λ.

V. RADIAL DRIFT VELOCITIES

Within the framework of our model the number of ions formed at any point in the discharge is a function only of the neutral-atom density and the electron temperature. These ions are generally considered to be formed solely by electron impact on neutral atoms or neutral metastables. Sze and Bennett[21] argue that the ion production rate should include ions formed by charge exchange, thereby leading to a different radial distribution of ions with no net radially directed velocity. Because we are mostly interested in the close-to-collisionless regime we lump all ion-formation processes together and assume that the random distribution of ion velocities is still Maxwellian. The effective production rate for ions (electron impact plus charge exchange) is treated as equivalent to the rate for electron impact only in the collisionless regime. Thus, although charge exchange interrupts the directed motion of ions, it does not distort the potential substantially from the TL form nor the formation rate from the rate given by Eq. (4). In any case, if one attempts to include the apparent effect of charge exchange on the radial ion distribution, one should also include the radially directed motion of neutrals which can persist after they are formed by neutralization of an ion or charge exchange.[8,9] The radial variation in radial ion drift velocity is, therefore, in the collisionless regime

$$v_r(r) = \frac{\int_0^r d\rho\, N_{\rho r} v_{\rho r}}{\int_0^r d\rho\, N_{\rho r}} , \tag{39}$$

where $v_{\rho r}$ is the radial velocity acquired by an ion in going from radius ρ to r. Explicitly,

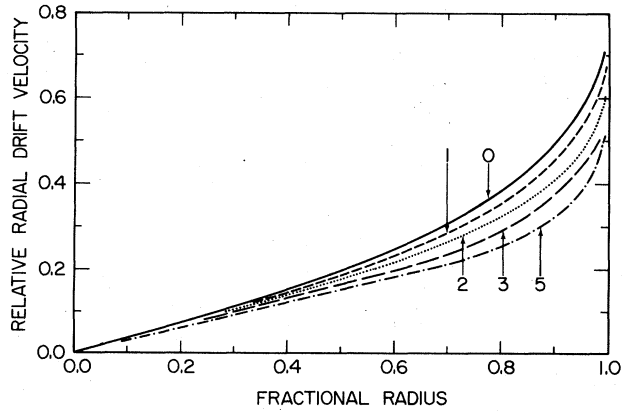

FIG. 5. Relative radial ion drift velocity as a function of radius in a cylindrical discharge with a Tonks-Langmuir radial potential.

$$v_r(r)=\left[\frac{2kT_e}{M}\right]^{1/2}\frac{\int_0^a dx\, xe^{V_x}}{\int_0^a dx\frac{xe^{V_x}}{(V_x-V_a)^{1/2}}}\,. \tag{40}$$

Collisions are included in Eq. (40) in a simple manner by the inclusion of a factor $\exp[-(R/\lambda)(x-a)]$ in both integrals. Some specific results from Eq. (40) in the case of a TL potential are shown in Fig. 5. These curves are in close qualitative agreement with curves given by Valentini.[8] Once again we do not use large values of the collision parameter as the close-to-collisionless regime is what interests us and where our model is appropriate.

Because the influence of the radial ion velocities on the transversely emitted line shapes has been the subject of several previous investigations,[14–17,21–23] we will not consider it further here.

VI. EFFECT OF DRIFT VELOCITIES ON LONGITUDINALLY EMITTED ION LINE SHAPES

As a result of the radial dependence of longitudinal ion drift velocity we expect the Doppler shift of ion-emission center frequencies to vary radially. If we assume that the Gaussian distribution of random longitudinally directed velocities is preserved in the presence of a longitudinal field, then the emitted line shapes from different radial positions in the tube would, in the collisionless regime, be progressively blue shifted on moving from the tube axis to the wall. However, if light emitted in the axial direction from only a restricted annular region was collected, a symmetrical Voigt profile would be observed. If light emitted in the axial direction from the whole tube bore was observed, this would involve a series of superimposed Voigt profiles with a distribution of amplitudes and center frequencies reflecting the radial variation of ion density and longitudinal drift velocity. We would expect such a profile to be broader than a profile observed from a more restricted region of the bore. A profile observed in this way would suggest higher ion temperature than the true value.

A. Without radial motion

It is only because the predominant net directed velocity of the ions is toward the wall that we can assume the random component of the longitudinal ion velocity v_z remains Gaussian. If the predominant motion of the ions was in the longitudinal direction then, the longer the mean free path the more asymmetrical the distribution function over v_z would become. We can illustrate this by considering a one-dimensional uniform plasma with a field $E_{\|}$ applied.

We assume that ions are formed from neutral atoms at a uniform rate per unit volume. The distribution function of these ions, before they accelerate in the field, is

$$f_0(v_z)=\left[\frac{M}{2\pi kT_a}\right]^{1/2}\exp(-Mv_z^2/2kT_a)\,. \tag{41}$$

We consider ions found within a small region dz. For an ion formed with velocity v_z', after a time t its velocity will be

$$v_z=v_z'+\frac{eE_{\|}}{M}t\,. \tag{42}$$

Thus, if all these ions are observed, in the absence of collision, the emitted line shape will correspond to a velocity distribution

$$f(v_z)\propto\exp\left[-\frac{M}{2kT_a}(v_z-bt)^2\right], \tag{43}$$

where we have written $b=eE_{\|}M$ for the acceleration of ions in the field. However, collisions must be taken into account. An equilibrium situation could not exist without ion removal, as ions are being continuously formed. After a time t, an ion initially formed with velocity v' has traveled a total distance s. The probability of this ion actually being observed after time t is $e^{-s/\lambda}$ where λ is the ion mean free path, which we will initially assume is independent of ion velocity. For ions initially formed with velocity $v_z'\geq 0$ (in the direction of the applied field),

$$s=s_1=v_z't+bt^2/2\,. \tag{44}$$

For ions formed with velocity $v_z'<0$ there are two possibilities for the total distance traveled. For ions observed at time t with $v_z<0$,

$$s=s_2=-v_z't-bt^2/2\,. \tag{45}$$

If, however, $v_z\leq bt$, these ions must have originated with velocity $v_z'<0$ and have been decelerated by the field and then reversed direction. The total distance traveled by this group of ions is

$$s=s_3=v_z^2/b+bt^2/2-v_zt\,. \tag{46}$$

To calculate the overall velocity distribution we must consider these three groups of ions. It is worth pointing out that a group of ions formed within a velocity interval dv_z remain within this same velocity interval as they accelerate, although they do spread out in space. However, if a long enough region in the z direction is observed, this is not important. For the first group of ions the distribution function is

$$f_1(v_z)=\int_0^{v_z/b}\exp\left[-\frac{M}{2kT}(v_z-bt)^2\right]\times\exp[(-v_zt+bt^2/2)/\lambda]dt\ ,\quad \text{with } v_z\geq 0 \text{ and } \nu\leq\nu_0\ . \tag{47}$$

For the second group,

$$f_2(v_z)=\int_0^{\infty}\exp\left[-\frac{M}{2kT}(v_z-bt)^2\right]\times\exp[(v_zt-bt^2/2)/\lambda]dt\ ,\quad \text{with } v_z<0 \text{ and } \nu>\nu_0\ . \tag{48}$$

For the third group,

$$f_3(v_z)=\int_{v_z/b}^{\infty}\exp\left[-\frac{M}{2kT}(v_z-bt)^2\right]\times\exp[(v_zt-bt^2/2-v_z^2/b)/\lambda]dt\ ,\quad \text{with } v_z\geq 0 \text{ and } \nu\leq\nu_0\ . \tag{49}$$

Therefore, for example, the emission line shape on the red side of line center is, apart from a normalization constant,

$$g(\nu)\propto \operatorname{erfc}(-B/\sqrt{D})\,g_D(\nu)\exp(B^2/D)\ ,\quad \text{with } \nu\leq\nu_0\ , \tag{50}$$

where

$$D=\frac{eE_{\parallel}}{2M\lambda}+(4\ln 2)\left[\frac{eE_{\parallel}\nu_0}{Me\Delta\nu_D}\right]^2\ , \tag{51}$$

$$B=\left[\frac{c\Delta\nu_D}{2\nu_0\lambda}+(4\ln 2)\left[\frac{eE_{\parallel}\nu_0}{Mc\Delta\nu_D}\right]\right]\left[\frac{\nu-\nu_0}{\Delta\nu_0}\right]\ , \tag{52}$$

and $g_D(\nu)$ is the Gaussian line shape of the neutral atoms of full width at half maximum height (FWHM),

$$\Delta\nu_D=\frac{2\nu_0}{c}\left[\frac{2kT\ln 2}{M}\right]^{1/2}\ . \tag{53}$$

With some algebra it can be shown that the overall line shape of the one-dimensionally accelerated ions is, apart from a normalization constant,

$$g(\nu)\propto\begin{cases}\exp\left[(4\ln 2)(1+Q)\left[\frac{\nu-\nu_0}{\Delta\nu_D}\right]^2\right]\left\{1+\operatorname{erf}\left[[4\ln 2(1+Q)]^{1/2}\left[\frac{\nu-\nu_0}{\Delta\nu_D}\right]\right]\right\}g_D(\nu)\ , & \nu\leq\nu_0 \quad (54)\\ \exp\left[-4Q\ln 2\left[\frac{\nu-\nu_0}{\Delta\nu_D}\right]^2\right]+\left[\frac{1+Q}{1-Q}\right]^{1/2}\exp\left[(4\ln 2)(1-Q)\left[\frac{\nu-\nu_0}{\Delta\nu_D}\right]^2\right] & \\ \quad\times\left\{\operatorname{erf}\left[[4\ln 2(1-Q)]^{1/2}\left[\frac{\nu-\nu_0}{\Delta\nu_D}\right]\right]\right\}g_D(\nu),\ \nu\geq\nu_0\ , & (55)\end{cases}$$

where $Q=kT/eE_{\parallel}\lambda$ and $Q<1$.

Note that as $Q\rightarrow 0$ the line-shape function becomes

$$g(\nu)\propto 1+\operatorname{erf}\left[(4\ln 2)\left[\frac{\nu-\nu_0}{\Delta\nu_D}\right]\right]\ . \tag{56}$$

This is the same line-shape function that results from solving the collisionless Boltzmann equation appropriate to cylindrical geometry with no radial or azimuthal variation of the distribution function f, namely,

$$\frac{eE_{\parallel}}{m}\frac{\partial f}{\partial v_z}=ZN_e\left[\frac{M}{2\pi kT}\right]^{1/2}\exp\left[-\frac{Mv_z^2}{2kT}\right]\ , \tag{57}$$

where Z is the ionization rate and N_e is the electron density (assumed constant everywhere).

For $Q\geq 1$,

$$g(\nu)\propto\exp\left[-4Q\ln 2\left[\frac{\nu-\nu_0}{\Delta\nu_D}\right]^2\right]+\frac{2}{\pi^{1/2}}\left[\frac{Q+1}{Q-1}\right]^{1/2}F\left[[(4\ln 2)(Q-1)]^{1/2}\left[\frac{\nu-\nu_0}{\Delta\nu_D}\right]\right]g_D(\nu)\ ,\quad \text{with } \nu\geq\nu_0\ , \tag{58}$$

where $F(z)$ is Dawson's integral. In a typical ion laser $Q\simeq 0.3$ but may vary from 0.1 to 1.0.

The overall line shape given by Eqs. (54) and (55) or (54) and (58) becomes more asymmetric as $Q\rightarrow 0$, as can be seen from Figs. (6) and (7). For $Q>0.5$ the lines begin to look like symmetrical Gaussians, but become narrower than the undistributed Doppler-broadened line would be. This is not a real effect but results from our treatment of λ as independent of particle velocity. If the electric field $E_{\parallel}$ is set to zero, then Eq. (47) becomes

$$f(v_z)=\int_0^{\infty}\exp\left[-\frac{Mv_z^2}{2kT}\right]\exp\left[\frac{v_zt}{\lambda}\right]dt\ ,\quad \text{with } v_z\geq 0\ . \tag{59}$$

In these circumstances the distribution function must

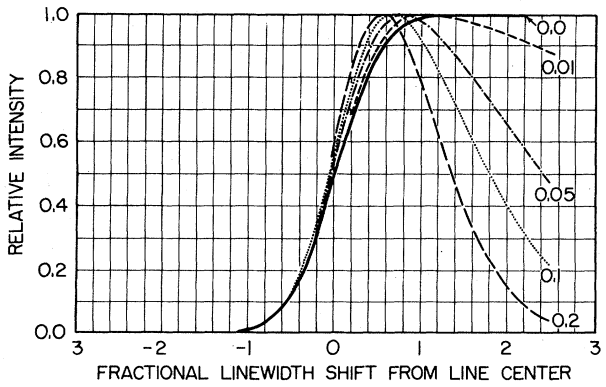

FIG. 6. Line shapes of ions accelerating from a Gaussian velocity distribution in a uniform electric field $E_{||}$ as a function of the relative mean-free-path factor $Q=kT/eE_{||}\lambda$, shown on each curve.

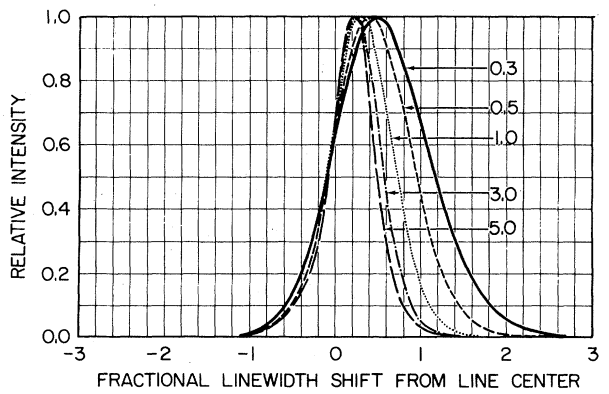

FIG. 7. Line shapes of ions accelerating from a Gaussian velocity distribution in a uniform electric field $E_{||}$ as a function of the relative mean-free-path factor $Q=kT/eE_{||}\lambda$, shown on each curve.

remain Maxwellian as ions are not accelerated after their formation from neutrals. Therefore, for the model to be consistent,

$$\frac{\lambda}{v_z}=\tau+E_{||}f(v_z)\,, \tag{60}$$

where τ is a constant. For $E_{||}=0$, Eq. (60) differs from the exact result for a single-component gas in which only motion along a single direction leads to collisions,[31] namely,

$$\frac{\lambda}{v_z}=\frac{Mv_z/kT}{\sqrt{\pi}N\sigma^2\psi[v_z(M/2kT)^{1/2}]}\,, \tag{61}$$

where N is the number density of particles with cross section σ (assumed velocity *independent*) and

$$\psi(x)=xe^{-x^2}+\sqrt{\pi}x^2(1+\mathrm{erf}x)\,. \tag{62}$$

As $v_z\to 0$ we can see that

$$\tau=\frac{1}{N\sigma^2}\left[\frac{2M}{\pi kT}\right]^{1/2}. \tag{63}$$

The difference between Eqs. (60) and (61) arises because in our one-dimensional model we are allowing empirically for a velocity-*dependent* cross section.

A mean-free-path variation with velocity of the form given in Eq. (60) prevents the anomalous narrowing of Doppler-broadened lines as $E_{||}\to 0$ predicted by Eqs. (54)—(56).

B. With radial motion

For ions which originate in an annulus $d\rho$ at radius ρ and drift radially to radius r, the contribution to the ion line shape emitted in the longitudinal direction is

$$[g(\nu)]_{\rho r}=N_{\rho r}\exp\{-[(2(\nu-\nu_0+\Delta_{\rho r})/\Delta\nu_D]^2\ln 2\}\,. \tag{64}$$

With an ion mean free path λ

$$N_{\rho r}=\frac{G_\rho\rho\,d\rho}{rv_{\rho r}}\exp\left[-\frac{R}{\lambda}\left[\frac{r}{R}-\frac{\rho}{R}\right]\right], \tag{65}$$

where v_ρ is given by Eq. (6). $\Delta_{\rho r}$ is the longitudinal Doppler shift acquired by this group of ions, observed in the direction opposite to the field

$$\Delta_{\rho r}=v_{z\rho r}\nu_0/c\,, \tag{66}$$

where ν_0 is the rest center frequency of the ion line. $v_{z\rho r}$ is the longitudinal drift velocity acquired by an ion which moves from ρ to r and is given by Eq. (17).

The total line shape observed from ions at radius r is

$$[g(\nu)]_r=\int_0^r d\rho\,\frac{N_\rho\rho}{rv_{\rho r}}\exp\left\{-\left[\frac{R}{\lambda}\left[\frac{r}{R}-\frac{\rho}{R}\right]+\{[2(\nu-\nu_0+\Delta_{\rho r})]/\Delta\nu_D\}^2\ln 2\right]\right\} \tag{67}$$

so, for a TL potential

$$[g(\nu)]_r=\int_0^a dx\,\frac{x\exp\left[V_x-\frac{R}{\lambda}(a-x)\right]}{[(1-x^2)^{1/2}-(1-a^2)^{1/2}]^{1/2}}$$

$$\times\exp\left\{-4\left[\left[\nu-\nu_0+\frac{A\nu_0}{c\sqrt{1.155}}\int_x^a\frac{dy}{[(1-x^2)^{1/2}-(1-y^2)^{1/2}]^{1/2}}\right]\frac{1}{\Delta\nu_D}\right]^2\ln 2\right\}, \tag{68}$$

where $A=(eE_{\|}R/M)(M/2kT_e)^{1/2}$.

The line shape observed if the entire tube bore is observed is, apart from a normalization constant,

$$g(\nu)=\int_0^a g(\nu)a\,da\ . \tag{69}$$

The line shapes predicted by Eqs. (68) and (69) become markedly more asymmetric as the longitudinal electric field increases, as can be seen from Figs. 8–10. The evaluation of Eq. (68) was carried out by numerical integration with analytic evaluation of the contribution to the integrals near their endpoints where their integrands blow up. To obtain good numerical accuracy these computations are quite lengthy, even on a large computer.

The shape of these lines is a function of R/λ and the dimensionless drift velocity factor

$$F=\frac{A\nu_0}{c\,\Delta\nu_D\sqrt{1.155}}\ .$$

For a low power, small bore, argon ion laser with $R=1$ mm, $kT_e=2.5$ eV, $E_{\|}=300$ V m^{-1}, $\lambda=488$ nm, and $\Delta\nu_D=3.5$ GHz, $F=0.11$. An increase in axial field strength and/or tube diameter could easily raise F.

For values of $F\simeq 0.3$, line asymmetry is becoming quite apparent, as can be seen from Fig. 9. Such line asymmetries have been observed by Davis and Lindsay.[32] This confirms our belief that radial variations in axial drift velocity should be considered carefully when line-shape measurements are being used to determine plasma parameters in cylindrical gas discharges. Figures 8–10 also show the measured broadening of axially emitted ion line shapes over the originating neutral-atom distribution. For example, at $F=0.3$, $R/\lambda=0$ the lines are approximately 18% wider than neutral lines. At $F=0.5$, $R/\lambda=0$ they are approximately 39% wider, at $F=0.5$, $R/\lambda=1$ they are approximately 32% wider. These increased widths are quite consistent with experimental observations made on argon ion lasers. For example, Ballik *et al.*[24] see ion lines varying from 0.5% to 25% wider than the neutral lines depending on operating current and pressure. Sze and Bennett[21] see ion lines from 3% to 19% wider under similar operating conditions.

VII. CONCLUSIONS

The radial and longitudinal motion of ions in low-pressure, cylindrical discharge plasmas affects the shape of emitted ion line shapes. We have considered in detail how the longitudinal ion velocity varies with radial position in a low-pressure cylindrical gas discharge. Evaluations have been carried out for different relative ion drift velocity and mean-free-path conditions. They show that under typical conditions appropriate to ion laser operation, asymmetrical line shapes should be observed in the longitudinal direction. These line shapes become substantially broader than lines emitted from neutral species depending on the relative values of axial field strength, tube radius, electron temperature, and ion mean free path. The predictions of the theory presented here are in satisfactory agreement with experimental observations of plasma parameters in gaseous-ion-laser discharges.

APPENDIX: ION TRAJECTORIES

As we have stated previously, the ion trajectories we have been considering are assumed to be directed predominantly towards the wall. Thus, the probability of a collision is only a function of the radial distance traveled by a much more slowly longitudinally drifting ion. To justify the assumption that radial distance traveled is the dominant factor in determining whether collisions are important, specific ion trajectories in a TL potential combined with a weaker longitudinal field have been calculated.

The equations of motion of an ion starting at rest from radius ρ are

$$dz/dt=eE_{\|}t/M\ , \tag{A1}$$

$$dr/dt=[2e(\phi_\rho-\phi_r)/M]^{1/2}\ ,$$

$$dx/dt=(2kT_e/M)^{1/2}(V_x-V_a)^{1/2}\ . \tag{A2}$$

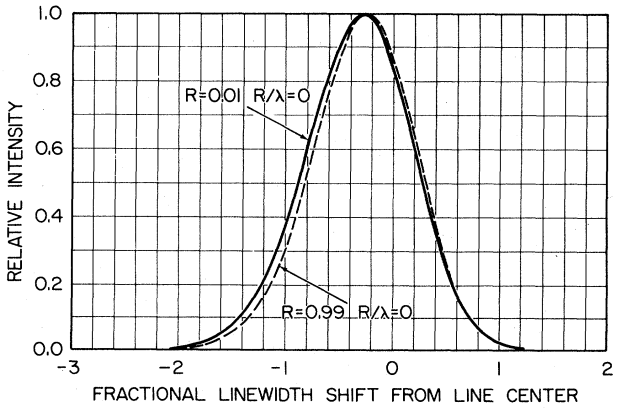

FIG. 8. Axially emitted ion line shapes observed from radial positions near the axis and wall in a cylindrical discharge where the ions move in a uniform axial field and a Tonks-Langmuir radial potential. The collisionless case with a drift velocity factor $F=0.3$ is shown.

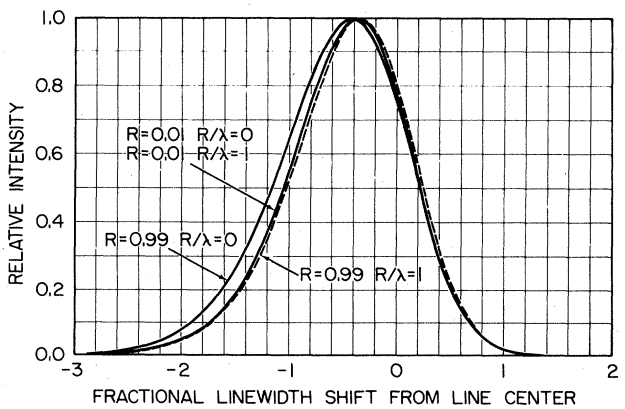

FIG. 9. Axially emitted ion line shapes observed from radial positions near the axis and wall in a cylindrical discharge where the ions move in a uniform axial field and a Tonks-Langmuir radial potential. Examples for the collisionless case and $R/\lambda=1$ are shown for a drift velocity factor $F=0.5$.

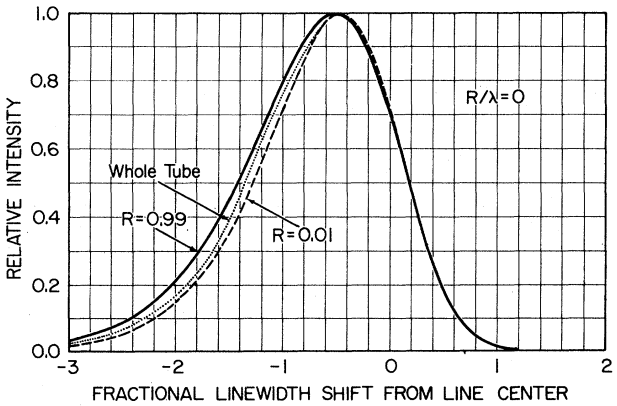

FIG. 10. Axially emitted ion line shapes observed from radial positions near the axis and wall and averaged over the tube bore in a cylindrical discharge where the ions move in a uniform axial field and a Tonks-Langmuir radial potential. The collisionless case with a drift velocity factor $F=0.7$ is shown.

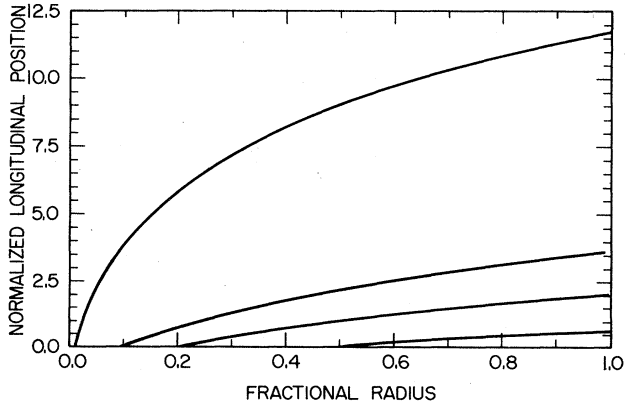

FIG. 11. Ion trajectories in a Tonks-Langmuir radial potential and a uniform axial electric field, shown for different starting radii.

t is the time the ion takes to travel from radius ρ to r. Integrating Eq. (A2) gives

$$t=\left[\frac{M}{2kT_e}\right]^{1/2}\int_x^a dy\frac{1}{(V_x-V_y)^{1/2}}\,. \tag{A3}$$

After this time the ion has moved radially from ρ to r and a longitudinal distance

$$\frac{z}{R}=\frac{eE_{\|}}{4kT_e}\left[\int_x^a dy\frac{1}{V_x-V_y}\right]^2 \tag{A4}$$

which for the TL potential gives

$$\frac{z}{R}=\frac{eE_{\|}R}{4.62kT_e}\left[\int_x^a dy\frac{1}{[(1-x^2)^{1/2}-(1-y^2)^{1/2}]^{1/2}}\right]^2. \tag{A5}$$

For a typical argon ion laser with $kT_e=4$ eV, $eE_{\|}=0.3$ eV mm^{-1}, and $R=1.5$ mm,

$$\frac{z}{R}\simeq 0.024\times\left[\int\cdots\right]^2. \tag{A6}$$

Figure (11) shows some typical trajectories calculated from Eq. (A5) where the longitudinal distance is normalized in units of $eE_{\|}R/(4.62kT_e)$. Even for an ion which starts near the tube axis, the maximum longitudinal drift will only be of the order of $R/4$, while for an ion formed halfway to the wall, the maximum longitudinal drift is only about $R/70$. The assumption of predominant radial motion is, therefore, entirely justified.

[1]L. Tonks and I. Langmuir, Phys. Rev. **34**, 876 (1929).
[2]J. V. Parker, Phys. Fluids **6**, 1657 (1963).
[3]J. R. Forrest and R. N. Franklin, J. Phys. D **1**, 1357 (1968).
[4]J. R. Forrest and R. N. Franklin, Brit. J. Appl. Phys. **17**, 1569 (1966).
[5]C. C. Davis and T. A. King, *Gaseous Ion Lasers,* in *Advances in Quantum Electronics, Vol. 2,* edited by P. W. Goodwin (Academic, London, 1973).
[6]K. G. Hernqvist and J. R. Fendley, Jr., IEEE J. Quantum Electron. **QE-3**, 66 (1967).
[7]H.-B. Valentini, Beitr. Plasmaphysik **23**, 51 (1983), and references therein.
[8]H.-B. Valentini, Beitr. Plasmaphysik **21**, 29 (1981).
[9]H.-B. Valentini, Beitr. Plasmaphysik **11**, 483 (1971); **12**, 88 (1972); **14**, 201 (1974).
[10]S. Torven, Phys. Scr. **4**, 65 (1971).
[11]J. H. Ingold, Phys. Fluids **15**, 75 (1972).
[12]S. A. Self and H. N. Ewald, Phys. Fluids **9**, 2486 (1966).
[13]C. E. Webb, J. Appl. Phys. **39**, 5441 (1968).
[14]Yu M. Kagan and V. I. Perel, Opt. Spektrosk. **2**, 298 (1957).
[15]Yu M. Kagan and V. I. Perel, Opt. Spektrosk. **4**, 3 (1958).
[16]Yu M. Kagan and V. I. Perel, Opt. Spektrosk. **4**, 258 (1958).
[17]Yu M. Kagan, Izv. Akad. Nauk SSSR, Ser. Fiz. **22**, 702 (1958).
[18]V. F. Kitaeva, Yu. I. Osipov, and N. N. Sobolev, Pis'ma Zh. Eksp. Teor. Fiz. **4**, 213 (1966) [JETP Lett. **4**, 146 (1966)]; IEEE J. Quantum Electron. **QE-7**, 391 (1971).
[19]V. F. Kitaeva, Yu I. Osipov, P. L. Rubin, and N. N. Sobelev, IEEE J. Quantum Electron. **QE-5**, 72 (1969).
[20]G. N. Mercer, V. P. Chebotaev, and W. R. Bennett, Jr., Appl. Phys. Lett. **10**, 177 (1967).
[21]R. C. Sze and W. R. Bennett, Jr., Phys. Rev. A **5**, 837 (1972).
[22]P. N. Zakharov and Yu A. Pekar, Sov. Phys. Tech. Phys. **15**, 1294 (1971) [Zh. Tekh. Fiz. **40**, 1664 (1970)].
[23]W. R. Bennett, Jr., E. A. Ballik, and G. N. Mercer, Phys. Rev. Lett. **16**, 603 (1966).
[24]E. A. Ballik, W. R. Bennett, Jr., and G. N. Mercer, Appl. Phys. Lett. **8**, 214 (1966).
[25]P. Zory, IEEE J. Quantum Electron. **3**, 390 (1967).
[26]F. A. Korolev, V. V. Lebedeva, A. I. Odintsov, and V. M. Salmon, Radio Eng. Electron. Phys. (USSR) **14**, 1318 (1969); **14**, 1519 (1969).
[27]F. A. Korolev, V. V. Lebedeva, A. E. Novik, and A. I. Odintsov, Opt. Spectrosc. (USSR) **33**, 435 (1972); **33**, 788

(1972).
[28]C. E. Webb and R. C. Miller, IEEE J. Quantum Electron. **QE-4**, 357 (1968).
[29]B. Van der Sijde, J. W. H. Dielis, and W. P. M. Graef, J. Quant. Spectrosc. Radiat. Transfer **16**, 1011 (1976).
[30]K. A. Karpov, *Tables of the Function* $F(z)=\int_0^z e^{x^2}dx$ *in the Complex Domain* (Macmillan, New York, 1964).
[31]J. Jeans, *An Introduction to the Kinetic Theory of Gases* (Cambridge University Press, Cambridge, England, 1962).
[32]C. C. Davis and S. M. Lindsay (unpublished).